Physica A 469 (2017) 681–694

Contents lists available at ScienceDirect

Physica A

journal homepage: www.elsevier.com/locate/physa

Fractal structures in the chaotic motion of charged particles in a magnetized plasma under the influence of drift waves

A.C. Mathias [a], R.L. Viana [a,*], T. Kroetz [b], I.L. Caldas [c]

[a] Department of Physics, Federal University of Paraná, Curitiba, Paraná, Brazil
[b] Department of Physics, Federal Technological University of Paraná, Pato Branco, Paraná, Brazil
[c] Institute of Physics, University of São Paulo, São Paulo, Brazil

HIGHLIGHTS

- Fractal structures are typically found in chaotic orbits of area-preserving dynamical systems, and they influence its transport properties.
- We identify a number of fractal structures in a problem of interest in plasma physics: the drift motion of charged particles in a magnetized plasma under the action of two drift waves.
- The fractal structures we identify are escape basins, describing its fractal basin structure and also the Wada property.

ARTICLE INFO

Article history:
Received 1 July 2016
Received in revised form 23 September 2016
Available online 19 November 2016

Keywords:
Fractal structures
Drift waves
Charged particle motion
Fractal basin boundaries
Exit basins
Wada property

ABSTRACT

Chaotic dynamics in open Hamiltonian dynamical systems typically presents a number of fractal structures in phase space derived from the interwoven structure of invariant manifolds and the corresponding chaotic saddle. These structures are thought to play an important role in the transport properties related to the chaotic motion. Such properties can explain some aspects of the non-uniform nature of the anomalous transport observed in magnetically confined plasmas. Accordingly we consider a theoretical model for the interaction of charged test particles with drift waves. We describe the exit basin structure of the corresponding chaotic orbit in phase space and interpret it in terms of the invariant manifold structure underlying chaotic dynamics. As a result, the exit basin boundary is shown to be a fractal curve, by direct calculation of its box-counting dimension. Moreover, when there are more than two basins, we verify the existence of the Wada property, an extreme form of fractality.

1. Introduction

One of the outstanding problems in modern plasma physics is the control of anomalous transport of particles across the magnetic field in fusion-oriented devices like tokamaks [1,2]. It is known that low-frequency drift-wave fluctuations govern plasma transport across magnetic field, specially in the plasma edge region [3]. These fluctuations arise from density and temperature gradients in a magnetized plasma, leading to ion and electron diamagnetic currents across the magnetic field. Drift waves are collective oscillations appearing due to the drift velocities associated with these currents [3].

* Corresponding author.
E-mail address: viana@fisica.ufpr.br (R.L. Viana).

http://dx.doi.org/10.1016/j.physa.2016.11.049
0378-4371/

Particle transport in high-temperature plasmas is dominated by the long-range electric field which results from the Coulomb interaction among charged particles. For magnetized plasmas the collective modes of interest are low-frequency ion acoustic oscillations, because they dominate transport properties, namely resistivity and thermal conductivity. The presence of steep density and temperature gradients causes instability of these low-frequency modes, leading to electrostatic turbulence and consequently an anomalous transport of particles and energy.

While the ion acoustic oscillations are related to the parallel component of wave vector (with respect to the magnetic field), its perpendicular component produces the $\mathbf{E} \times \mathbf{B}$ drift of particle guiding centers across the magnetic field [4]. The corresponding dynamical system can be described by a Hamiltonian, after the definition of suitable coordinates and momenta.

It has been found that the motion influenced by a single drift wave leads to an integrable system [5]. The presence of KAM tori (invariant curves, in the Poincaré surface of section) prevents particle diffusion, resulting in a localized motion within "convection cells". However, if two or more drift waves are considered the system is no longer integrable and chaotic motion is a possible outcome. This chaotic dynamics can be viewed as a low-dimensional approximation of the extremely complicated scenario observed in electrostatic turbulence [6].

The mathematical properties underlying chaotic orbits in area-preserving dynamical systems lead to the appearance of fractal structures which make transport highly non-uniform through the chaotic orbit. One of such structures is the exit or escape basin, which is a region in phase space defined by the set of initial conditions that escape, or exit, outside a prescribed region of the phase space [7]. In open Hamiltonian systems such exits can be literally openings through which trajectories can escape, such as billiards with holes, as in Ref. [8]. In other systems the exits can be thought as regions to which trajectories collide and are considered lost [9]. Also, it would be an open equipotential surface consisting of channels through which an orbit can escape [10].

The latter is the case when we consider charged particles in a magnetic field under the action of two drift waves. In the non-integrable case particles can follow chaotic orbits which intersect exits such as plates or the wall itself which contains the particles. Once particles hit those exits they are considered lost and removed from numerical simulations. We are particularly interested in the structure of those exit basins in the case we can vary at least some parameters like the amplitude of the second wave, related to the degree of non-linearity present in the system.

If the boundary between two basin were a smooth curve it would be simple, in principle, to determine to what exit a given initial condition will asymptote to. However, for two exit basins in the chaotic region the boundary is typically fractal, which is by itself a factor limiting the knowledge we have to predict the final state of the system [11]. This uncertainty is ultimately determined by the box-counting dimension of the fractal boundary. Fractal basin boundaries have been long investigated in a variety of dissipative as well as conservative systems [12]. Moreover, we included in this paper an application of a very recent method proposed by Daza et al., which introduces the concept of a basin entropy so as to analyze fractal structures in the basin boundaries [13].

If more than two exit basins are present, there follows that the corresponding exit basins can exhibit the even stronger Wada property: any point which is on the boundary of one escape basin is also simultaneously on the boundary of all the others [14]. The Wada property has been investigated in many open Hamiltonian systems, as the three-disk billiard [15], Duffing equation [16–18], particle scattering by a Hénon–Heiles potential [19,20], tracer advection in fluid flows [21,22], and quasi-periodically driven systems [23]. The occurrence of Wada basins can be quantitatively characterized by a grid approach [24]. In the plasma physics context, fractal and Wada basins have been described for the magnetic field line flow in time-independent systems [25–28].

The major goal of this manuscript is to present some of these fractal structures and the role they play in the passive transport of particles in the chaotic motion of guiding centers experiencing $\mathbf{E} \times \mathbf{B}$ drift influenced by more than one drift wave. By considering this as an open system, many structures are related to the non-uniform escape of particles through different exits both inside and at the boundary of the plasma. In a previous work [29] the presence of fractal structures in the phase space of dissipative drift motion was considered, showing the existence of fractal basin boundaries for attractors that appear due to the presence of small damping. In this paper, on the other hand, we consider the conservative version of the problem, showing that these fractal structures can be assigned also to the escape properties of the chaotic orbit.

This paper is organized as follows: in Section 2 we outline the model for particle motion in drift waves to be used. Section 3 presents numerical results for chaotic particle motion with emphasis on chaotic motion. Section 4 considers fractal structures for two escape basins, particularly their fractal basin boundaries. Section 5 explores topological properties like the existence of Wada basins for three (or more) escape basins. Our Conclusions are left to the final Section.

2. Particle–drift wave interaction model

One approach to describe the turbulent behavior at the tokamak plasma edge related to drift instabilities is to investigate single particle motion in presence of both magnetic and electric fields, the latter being perturbed by electrostatic drift waves. Factoring out the gyration around magnetic field lines we can focus on the $\mathbf{E} \times \mathbf{B}$ drift motion of the guiding centers.

Neglecting curvature effects the plasma edge region can be approximately described by a slab geometry: let z be the toroidal direction, along which there is a uniform magnetic field $\mathbf{B} = B_0\hat{\mathbf{z}}$. The radial direction is described by the x coordinate, parallel to a radial electric field perturbed by one or more electrostatic drift waves. The drift current, on its hand, has the poloidal direction described by y coordinate, with periodicity 2π. Hence the plasma is bounded in x and periodic in y.

We assume that the ion and electron charges do not affect appreciably the electric and magnetic fields, hence the corresponding guiding centers can be considered as passive tracers, or test particles. Such a test particle moves with the $\mathbf{E} \times \mathbf{B}$ drift velocity

$$\mathbf{v} = -\frac{\nabla \Phi \times \mathbf{B}}{B^2}, \tag{1}$$

where the electric field is written as $\mathbf{E} = -\nabla \Phi$, where $\Phi(x, y, t)$ is a scalar potential. This is equivalent to the following set of canonical equations

$$v_x = \frac{\mathrm{d}x}{\mathrm{d}t} = -\frac{1}{B_0}\frac{\partial \Phi}{\partial y}, \tag{2}$$

$$v_y = \frac{\mathrm{d}y}{\mathrm{d}t} = \frac{1}{B_0}\frac{\partial \Phi}{\partial x}, \tag{3}$$

corresponding to a time-dependent Hamiltonian

$$H(x, y, t) = \frac{1}{B_0}\Phi(x, y, t). \tag{4}$$

The electric potential can be divided into two parts: an equilibrium part $\Phi_0(x)$ corresponding to a radial electric field and a perturbation caused by N drift waves with amplitudes A_i, frequencies ω_i and wave vectors $\mathbf{k}_i = (k_{xi}, k_{yi})$, for $i = 1, 2, \ldots, N$, in such a way that [5]

$$\Phi(x, y, t) = \Phi_0(x) + \sum_{i=1}^{N} A_i \sin(k_{xi}x)\cos(k_{yi}y - \omega_i t), \tag{5}$$

where we suppose that there is a stationary wave pattern along the radial distance x and a traveling wave along the poloidal direction y. Let L_x and L_y the characteristic lengths along both directions (L_x may stand for the radial extent of the plasma edge region and L_y is the rectified poloidal circumference), hence

$$k_x = \frac{n\pi}{L_x}, \qquad k_y = \frac{2\pi m}{L_y}$$

where m and n are suitably chosen positive integers.

In the case of N drift waves the Hamiltonian reads

$$H(x, y, t) = \frac{1}{B_0}\left\{\Phi_0(x) + \sum_{i=1}^{N} A_i \sin(k_{xi}x)\cos(k_{yi}y - \omega_i t)\right\}. \tag{6}$$

The electric field in a tokamak has typically a monotonic radial profile

$$\Phi_0 = \alpha x^2 + \beta x, \tag{7}$$

where the parameters α and β can be adjusted to fit the electric potential profile of a tokamak discharge [30,31]. In particular, if $\alpha = 0$ we have that $\beta = E_0$ represents a uniform electric field in the radial direction.

For two drift waves ($N = 2$), using dimensionless variables and in the reference frame moving with the phase velocity of wave 1 the normalized Hamiltonian (6) is given by

$$H(x, y, t) = \Phi_0(x) - u_1 x + A_1 \sin(k_{x1}x)\cos\left(k_{y1}y\right) + A_2 \sin(k_{x2}x)\cos\left[k_{y2}(y - ut)\right], \tag{8}$$

where $u_1 = \omega_1/k_{y1}$ is the phase velocity of the first wave and

$$u = \frac{\omega_2}{k_{y2}} - \frac{\omega_1}{k_{y1}} \tag{9}$$

is the difference between the phase velocities of the two waves.

Let us first consider the case of only one wave ($A_2 = 0$). Since $H = H(x, y)$ the system is integrable (in the Liouville sense). In this case the phase space has cells where the particle motion is bounded. It can be defined a dimensionless trapping parameter as

$$U(x) = \frac{1}{A_1 k_{x1}}\left(\frac{\mathrm{d}\Phi_0}{\mathrm{d}x} - u_1\right), \tag{10}$$

which is proportional to the difference between the drift velocity (1) and the phase velocity of the wave. It quantifies how sensitive is the equilibrium system with respect to a second drift wave, and how intense we expect to be the radial particle transport [31].

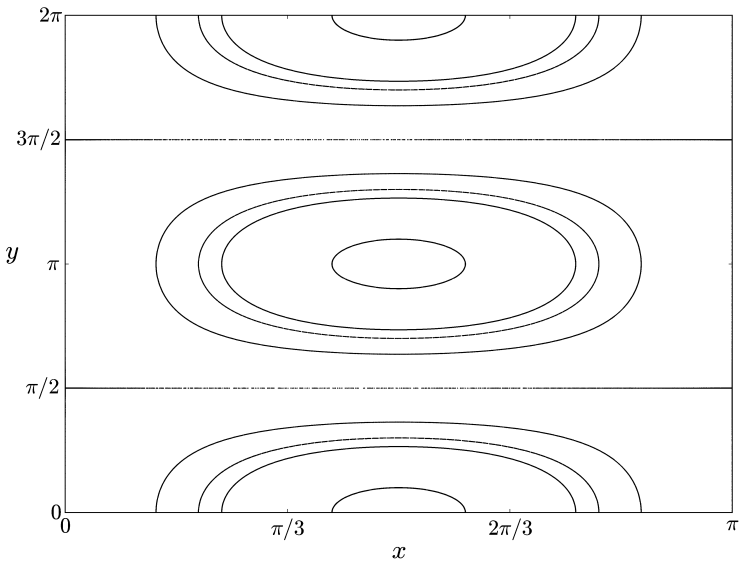

Fig. 1. Phase portrait for the Poincaré time-$T = 2\pi$ map, in the case $A_2 = 0$ and $U = 0$.

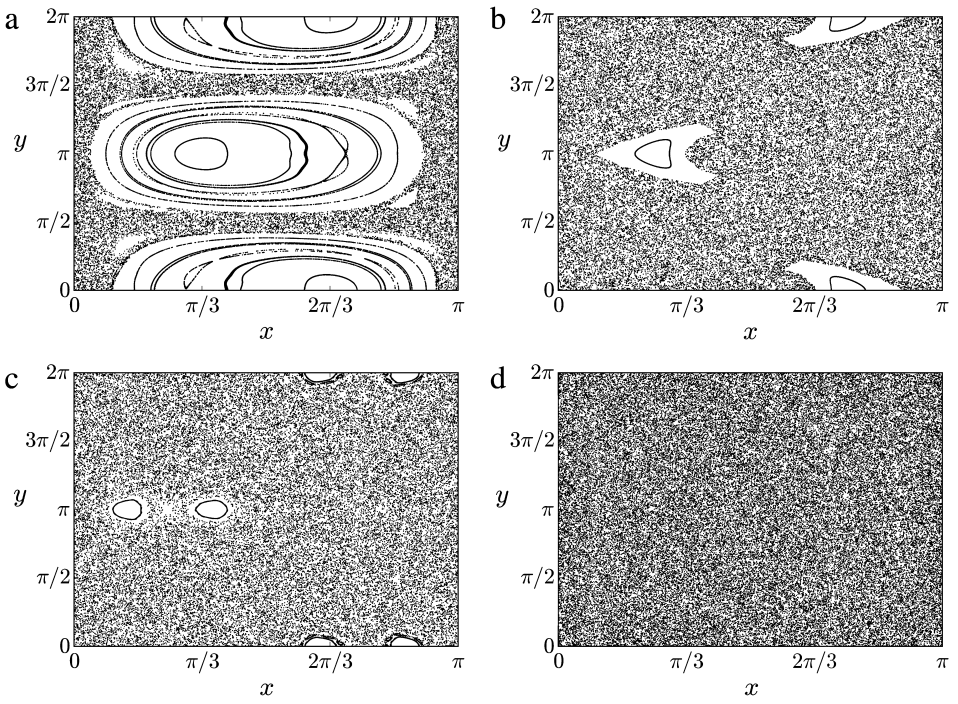

Fig. 2. Phase portrait for the Poincaré map, in the case $U = 0$ and different values of the parameter A_2. (a) 0.1, (b) 0.5, (c) 1.5, and (d) 2.0.

The canonical Eqs. (2)–(3) were numerically integrated for Hamiltonian (8), using an Adams 12th-order predictor–corrector scheme, and a Poincaré map was taken after considering only the values of (x, y) at times equal to an integer multiple of the period $T = 2\pi$ (stroboscopic map). We use the following values for the system parameters

$$\omega_1 = 0.2, \qquad \omega_2 = 1.2, \qquad k_{x1} = k_{y1} = k_{x2} = k_{y2} = 1.0, \qquad u = 1.0, \qquad A_1 = 1.0, \qquad U = 0.0,$$

and take A_2 (amplitude of the second wave) as a tunable parameter. The integrable case ($A_2 = 0$) is depicted in Fig. 1, where we observe the cells in which the particle motion is bounded. These cells are limited by separatrices emanating from hyperbolic fixed points at $(x = 0, \pi)$ and $y = \pi/2, 3\pi/2$. The closed curves orbit around the elliptic fixed points at $x = \pi/2$ and $y = 0, \pi, 2\pi$.

When the amplitude of the second wave is small but nonzero [Fig. 2(a)] the system integrability is broken, and the interior of the cells has a more involved structure, the former separatrices intersecting at an infinite number of

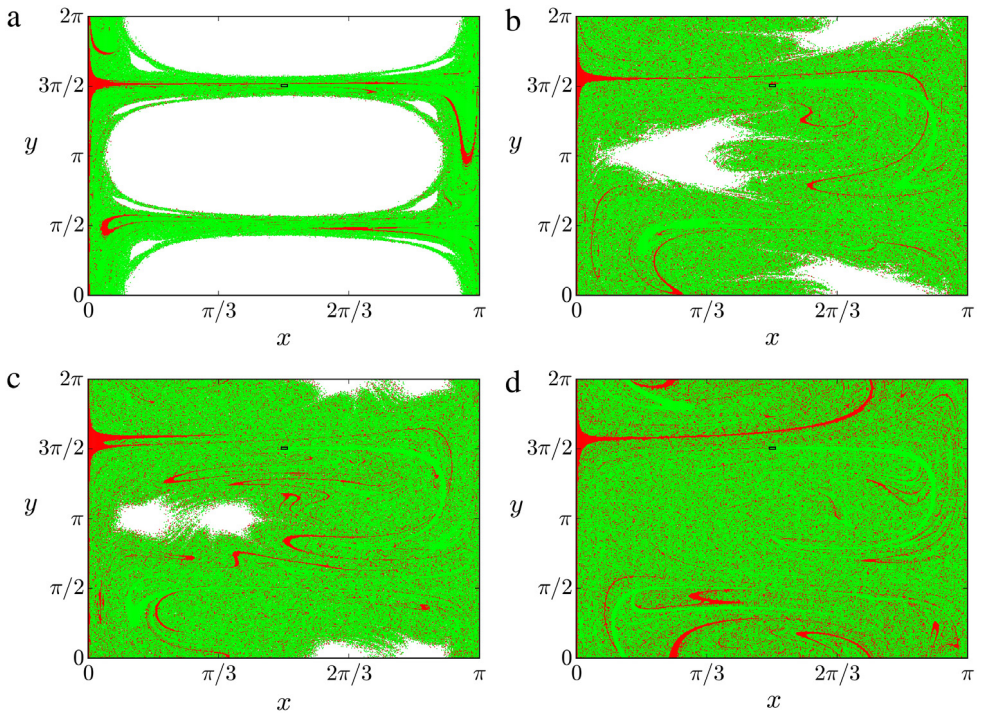

Fig. 3. Exit basins for the wall ($x = 0$, red points) and a small square box with center at $x = \pi/2$ and $y = 3\pi/2$ and width 0.05 (green points) in the case $U = 0$ and different values of the parameter A_2. (a) 0.1, (b) 0.5, (c) 1.5, and (d) 2.0. (For interpretation of the references to color in this figure legend, the reader is referred to the web version of this article.)

homoclinic/heteroclinic points, which are the skeleton of the area-filling chaotic orbit. Increasing the control parameter A_2 causes the destruction of most invariant curves around the displaced elliptic points, and the consequent enlargement of the chaotic orbit [Fig. 2(b)]. A further increase of A_2 leads to a bifurcation of the elliptic points, turning them to hyperbolic points and creating two new elliptic points (a saddle-center bifurcation) [Fig. 2(c)]. Finally, as A_2 is large enough, no visible traces of the invariant curves remain and the chaotic region spans virtually all phase space [Fig. 2(d)].

3. Exit basins

The dynamics in the chaotic orbits displayed in Fig. 2 is aperiodic but not uniformly so, due to the complicated nature of the manifold structure therein. This non-uniformity of chaotic motion can be illustrated by the structure of escape (or exit) basins, which is a phase space region defined by the set of initial conditions that escape, or exit, outside a prescribed region of the phase space. For example, if we consider that particles hitting the surface $x = 0$ (physically corresponding to a "wall") are lost, we might be interested on the basin of escaping initial conditions to that wall. Another possibility is that a chaotic orbit hits a given "opening" within the phase space (an exit window) before it hits the wall. Then we can draw the basin of escaping initial conditions through that exit [7]. If the initial condition is not placed in the chaotic region (if it belongs to the interior region of a periodic island, for example) it generates a non-escaping orbit and do not belong to any exit basin.

In summary, for an initial condition originating in a chaotic region in the phase space there are three possibilities: (i) either the particle hits the wall at $x = 0^+$ (i.e. within a given tolerance) and is considered lost; (ii) or the particle hits first a bounded region (window) and is also considered as lost, or (iii) it never escapes. As a matter of fact, there exists a Lebesgue measure zero set of initial conditions for which the trajectories never leave the chaotic region, but the probability of a typical trajectory to belong to this set is zero [12].

Fig. 3 shows a representation of the exit basins for the wall at $x = 0$ (red points) and an opening represented by a small square box which center is placed at $x = \pi/2$ and $y = 3\pi/2$, with width $w = 0.05$ (green points). The initial conditions that never escape through these regions are left blank. These exit basins have an involved structure for all values of the control parameter A_2 [Fig. 3(a)–(d)]. The smaller size of the red basin, when compared with the green basin, can be explained qualitatively on the basis of the $\sin x$ dependence of the x-component of the particle velocity. Since the latter tends to zero as $x \to 0$, it is more probable that a particle be lost through the square opening than through the wall $x = 0$.

Another factor that influences the relative sizes of the two exit basins is the width of the opening inside the chaotic region [27]. For example, in Fig. 4 the width has increased to $w = 0.15$, causing an increase of the area of the green basin, with respect to the area occupied by the red basin. We have computed these areas through the fraction of the basin points with respect to the total number of grid points in which the phase portrait has been divided. In particular, we have done so

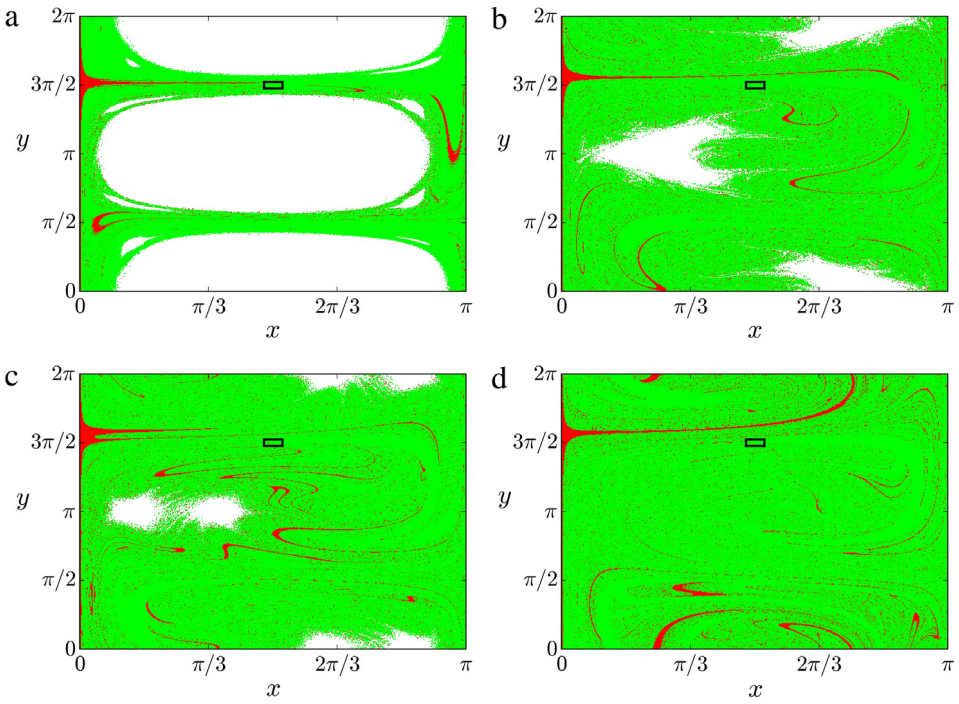

Fig. 4. Exit basins for the wall ($x = 0$, red points) and a small box with width 0.15 (green points) in the case $U = 0$ and different values of the parameter A_2. (a) 0.1, (b) 0.5, (c) 1.5, and (d) 2.0. (For interpretation of the references to color in this figure legend, the reader is referred to the web version of this article.)

for the points belonging to the red basin, i.e. we computed the fraction S_{wall} of initial conditions which lead to trajectories hitting first the wall.

Our results are presented in Fig. 5 in terms of A_2, for two different values of the exit width w. As a trend, Fig. 5(a) indicates that the red exit basin area increases with the intensity of the second wave. This can be explained by remembering that the increase of A_2 actually causes the enlargement of the chaotic orbit itself [see Fig. 2], and thus the available number of initial conditions for trajectories hitting either exit. On the other hand, the red basin area decreases with the width of the second exit for the same value of A_2 [Fig. 5(b)], since the more initial conditions belong to the green basin, the less initial conditions are expected to belong to the red basin (those are the only available exits). Such observations can be explained by a detailed analysis of the invariant manifold structure, as it will be made in the next section.

It is worth to explore some physical consequences of the increase of the red basin area with the value of A_2. A cursory look at Figs. 3 and 4 shows that most of the initial conditions placed in the chaotic region of the phase space belong to the green basin, i.e. they escape by the small box placed inside the chaotic region. Hence many particles belonging to the red basin, specially those far from the tokamak wall (by where they escape), spend a relatively large time in the chaotic region, and are expected to be more energetic than particles that escape rapidly by the small box. The increase of the red basin area with A_2 suggests that the intensity of the second drift wave increases also the transport of energetic particles through the tokamak wall. This result agrees with experimental measurements of turbulent-driven particle fluxes through the plasma edge of tokamaks, which increase with the turbulence level [32].

4. Invariant manifolds and exit basin structure

The nature and properties of the exit basins discussed in the previous section can be understood from the structure of the chaotic region in phase space, which is governed by its invariant manifold structure. Let the Poincaré map obtained from the numerical integration of the Hamilton's equations for the drift trajectories (2)–(3) be denoted as **F**, which is invertible (since we can integrate the equations backwards by using negative stepsizes). Due to the area-preserving nature of the system the map **F** is symplectic. We assume the existence of an area-filling chaotic orbit due to the non-integrability of the underlying Hamiltonian system.

Let P be an unstable periodic point of the map **F** embedded in this chaotic region. The stable and unstable subspaces for P are denoted as $E^s(P)$ and $E^u(P)$, respectively, and are eigendirections for the tangent map $\mathbf{DF}(P)$, with real eigenvalues $|\xi_s| < 1$ for $E^s(P)$ and $|\xi_u| > 1$ for $E^u(P)$. These subspaces are tangent to the stable ($W^s(P)$) and unstable ($W^u(P)$) manifolds at P. The invariant manifolds $W^u(P)$ and $W^s(P)$ can be numerically obtained by considering the number of forward and

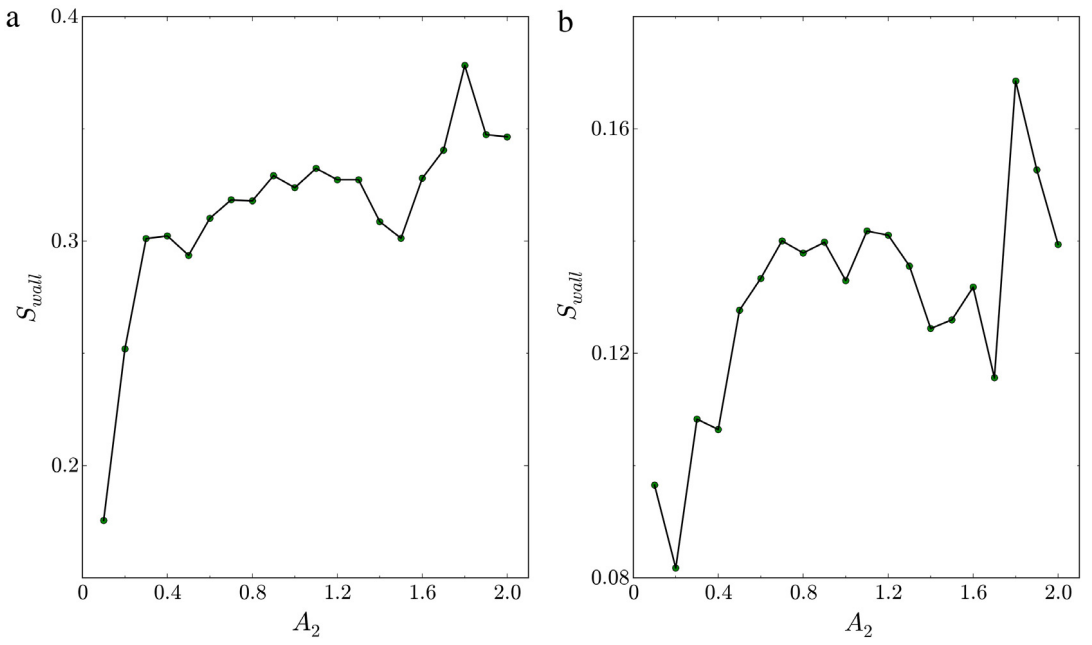

Fig. 5. Fraction of the red exit basin area S_{wall} as a function of A_2 for different values of the exit width w. (a) 0.05 and (b) 0.15. (For interpretation of the references to color in this figure legend, the reader is referred to the web version of this article.)

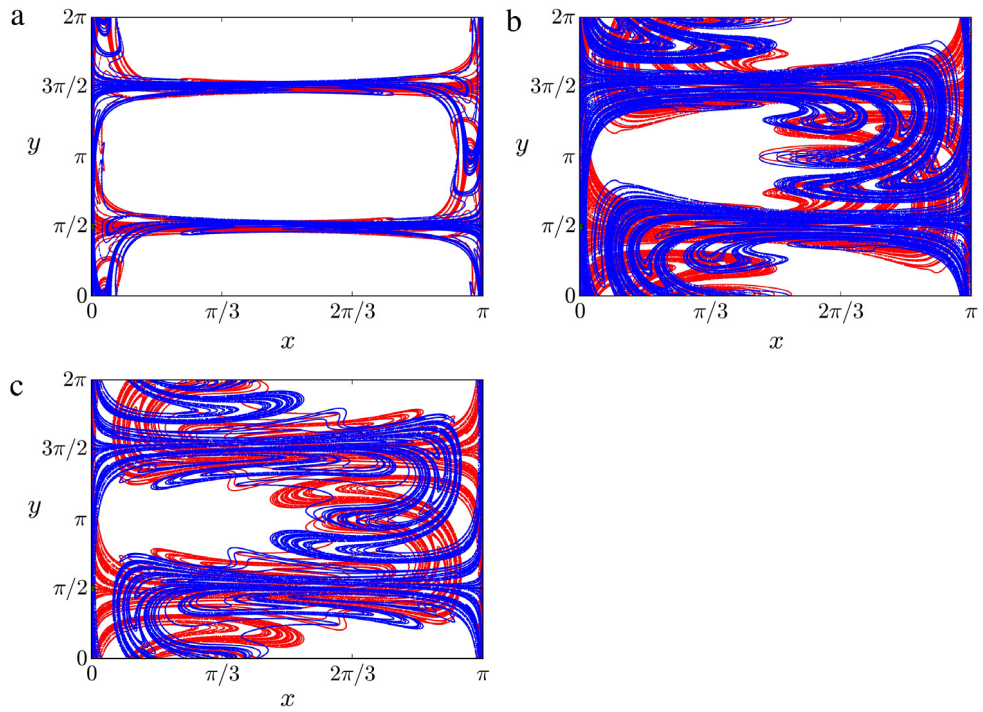

Fig. 6. Unstable (red curve) and stable (blue curve) invariant manifolds of an unstable fixed point embedded in the chaotic orbit for different values of A_2. (a) 0.1, (b) 0.5, and (c) 1.5. (For interpretation of the references to color in this figure legend, the reader is referred to the web version of this article.)

backward images, respectively, of a small ball filled with a large number of initial conditions and centered at a numerical approximation for the location of an unstable periodic orbit P embedded in the chaotic orbit [Fig. 6].

The increasingly higher region occupied by those manifolds is reflected the increased area of both red and green basins in Fig. 3. The striations displayed by the manifold branches explain the incursive fingers characterizing pieces of the exit basins and which act as escape channels through which chaotic trajectories are directed towards either the wall or the rectangular

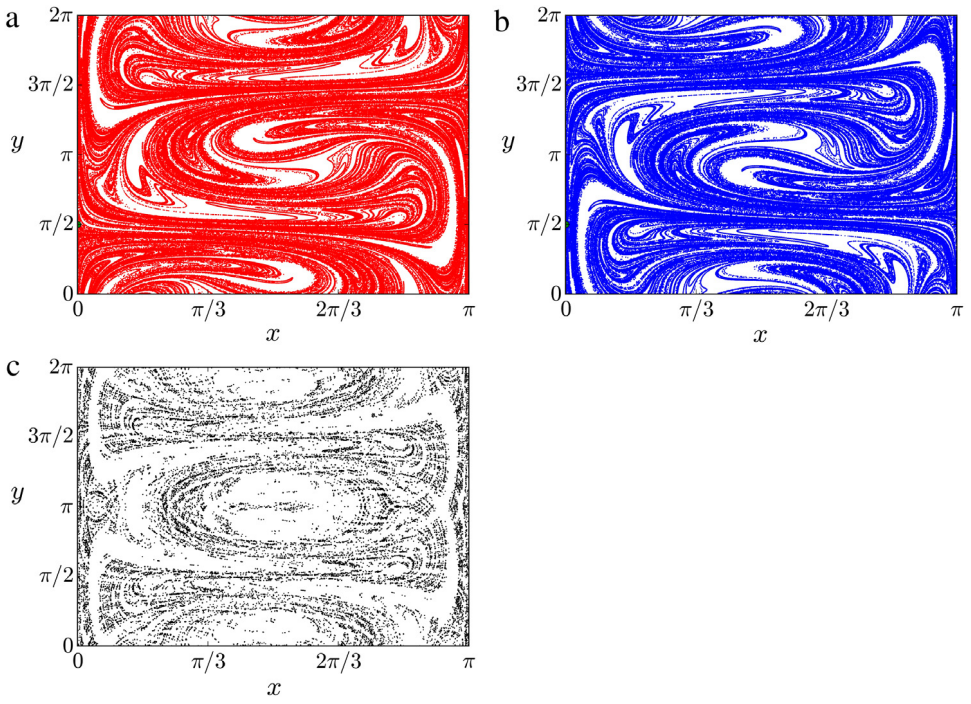

Fig. 7. Unstable (a) and stable (b) manifolds stemming from an unstable periodic orbit embedded in the chaotic region for $A_2 = 2.0$. The corresponding chaotic saddle is depicted in (c).

exit. The wider is the exit the more unstable manifold segments will cross this exit, leading to trajectories escaping by that exit. Hence, the size of that exit ultimately causes an increase of the corresponding exit basin. This has physical consequences similar to those caused by the increase of the second wave amplitude, as discussed at the end of the previous section.

The skeleton of the chaotic orbit is a chaotic saddle, formed by homoclinic and heteroclinic intersections of the stable and unstable manifolds of an infinite number of unstable periodic orbits embedded in the chaotic region, and which support the ergodic measure of typical orbits [22]. In other words, a chaotic saddle is a non-attracting invariant set with a dense chaotic orbit. Initial conditions belonging to this saddle remain in the chaotic region, unless portions of the saddle intercept the exit regions. Fig. 7(c) shows a numerical approximation of the chaotic saddle resulting from the intersection of the stable and unstable manifolds depicted in Fig. 7(a) and (b), respectively. The existence of a chaotic saddle is a further confirmation of the fractal nature of the exit basin boundaries.

5. Fractal exit basin boundaries

The complicated structure of the exit basins is qualitatively explained by the convoluted nature of the invariant manifolds comprising the infrastructure of the chaotic orbit, mathematically represented by the chaotic saddle. In addition we can also make a quantitative study of the exit basin boundaries by the uncertain fraction method. The key issue is that the boundaries separating two exit basins have final state sensitivity [33].

An initial condition in the phase space is known up to a given uncertainty ε, what can be represented by a ball of radius ε centered at that initial condition. If the initial condition is so near the boundary that the ε-ball intercepts it, we cannot be sure if that initial condition will evolve to one or another exit. The union of all ε-balls intercepting the boundary, divided by the area of the phase space region, is called the uncertain fraction $f(\varepsilon)$. If the boundary is smooth we have that $f(\varepsilon) \sim \varepsilon$, since the uncertain conditions occupy a strip of width 2ε straddling the boundary.

On the other hand, for fractal basin boundaries, the uncertain fraction scales as $f(\varepsilon) \sim \varepsilon^{\alpha}$, where $0 < \alpha < 1$ is the uncertainty exponent. The latter is related to the box-counting boundary dimension d by $\alpha = 2 - d$, in a two-dimensional phase space [12]. The more involved the basin boundary, the higher is its box-counting dimension such that it can be used as a quantitative characterization of the basin structure complexity [11].

We can examine, for example, the influence of the amplitude of the second wave on the basin structure by computing the uncertain fraction for different values of A_2 [Fig. 8]. We selected a representative portion of the exit basin boundaries in Fig. 2 and covered it with a fine mesh of initial conditions. At each initial condition **A** we randomly choose three other initial conditions $\mathbf{B}_1$, $\mathbf{B}_2$, and $\mathbf{B}_3$, inside an ε-ball centered at **A**. If **A** and $\mathbf{B}_{1,2,3}$ lead to orbits escaping through different exits, it turns out that **A** a ε-uncertain initial condition. The uncertain fraction was estimated from the ratio between the number of all uncertain conditions and the total number of mesh points. The uncertainty exponent was obtained from a least-squares fit

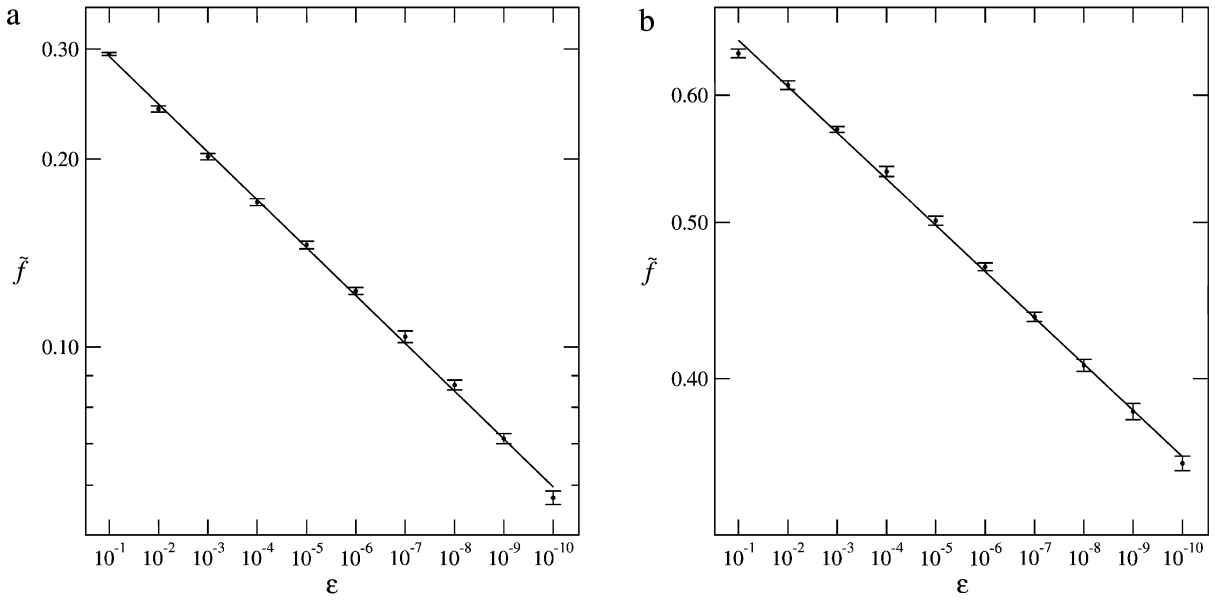

Fig. 8. Uncertain fraction as a function of the uncertainty radius for the exit basin boundary with different values of A_2. (a) 0.1 and (b) 2.0. The box width is $w = 0.05$.

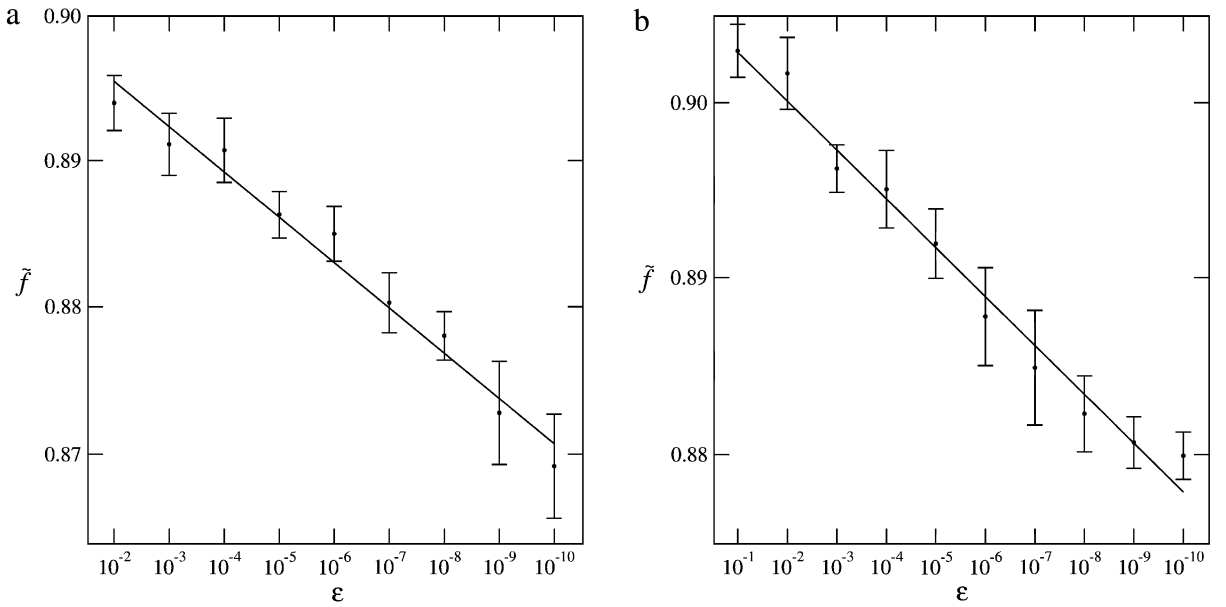

Fig. 9. Uncertain fraction as a function of the uncertainty radius for the exit basin boundary with different values of A_2. (a) 0.1 and (b) 2.0. The box width is $w = 0.15$.

in a log–log plot of $f(\varepsilon)$ *versus* ε for different values of A_2, comprising ten orders of magnitude. For smaller A_2 the exit basin boundary dimension is $d \approx 1.92$ [Fig. 8(a)], whereas a larger value of A_2 yields $d \approx 1.97$, hence a slightly more complex basin structure [Fig. 8(b)].

The same technique was used to investigate the effect of increasing opening width on the basin dimension. For $w = 0.15$ we show in Fig. 9(a) and (b) that the boundary dimension is $d \approx 1.99$ for two widely different amplitudes showing that, although the exit basin area is affected by the exit width [see Fig. 5] the corresponding exit boundaries do not show appreciable effect.

In addition, we can apply to this problem a technique introduced by Daza et al., based on the calculation of the so-called called basin entropy, which is a quantitative measure of the degree of uncertainty achieved by the fractality of the basin boundary [13]. The basic idea of this technique is to make a grid in a given region of the phase space, such that each grid

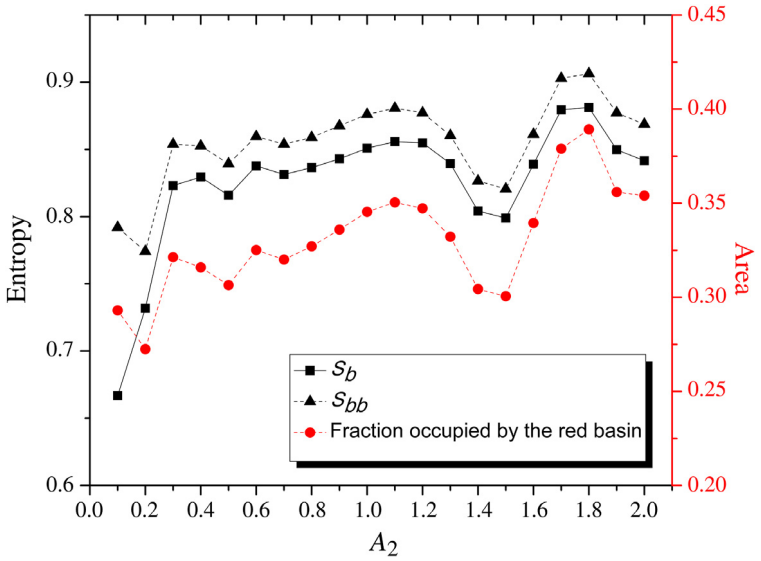

Fig. 10. Basin entropy and basin boundary entropy for the case of two exits [see Fig. 3] as a function of the second wave amplitude. We also plot the fraction occupied by the red basin. (For interpretation of the references to color in this figure legend, the reader is referred to the web version of this article.)

point can be assigned to a random variable with the different exits (in the present context) as the possible outcomes. The basin entropy results from applying the Gibbs entropy definition to that set.

More precisely, let a region Ω of the phase space characterized by the presence of N_A exits (or attractors, in its dissipative version). The region Ω is covered by a fine mesh of boxes with size ε, and to each initial condition we assign a color labeled from 1 to N_A. The colors within each box are randomly distributed according to a probability $p_{i,j}$ for the jth color assigned to the ith box. On supposing that the trajectories inside a box are statistically independent we compute the Gibbs entropy of the ith box as [13]

$$S_i = \sum_{j=1}^{m_i} p_{i,j} \log\left(\frac{1}{p_{i,j}}\right), \tag{11}$$

where $m_i \in [1, N_A]$ is the number of colors inside the ith box. The total entropy of the grid is the sum over the N boxes, or $S = \sum_{i=1}^{N} S_i$, such that the basin entropy is the total Gibbs entropy divided by the number of boxes, $S_b = S/N$. For a single attractor the basin entropy is zero, meaning zero uncertainty, whereas for N_A equiprobable exits $S_b = \log N_A$, which means a completely randomized basin structure.

We may be interested in the uncertainty related to the basin boundary, rather than the uncertainty of the whole basin structure, as quantified by S_b. For this purpose we can repeat the above calculation, but restricting the computation of the total entropy to the number N_b of boxes which contain more than one color, yielding the so-called boundary basin entropy, or $S_{bb} = S/N_b$.

Applying those concepts to the escape basin structure of the present paper, let us consider the case of two exits, namely the wall at $x = 0$ (red points) and a small square box with center at $x = \pi/2$ and $y = 3\pi/2$ and width 0.05 (green points). We considered a grid of 1000×1000 points of each basin, distributed inside 4×10^4 boxes. For each grid point, a maximum number of 3000 stroboscopic map points were computed, excluding from the statistics those initial conditions that have not escaped during that integration time. For each box we obtained the quantities

$$p_1 = \frac{n_1}{n_1 + n_2}, \qquad p_2 = \frac{n_2}{n_1 + n_2},$$

where n_1 is the number of points of the box corresponding to the exit 1, and n_2 is the number for exit 2. The entropy for each box is

$$S = -p_1 \log(p_1) - p_2 \log(p_2),$$

and the basin entropy S_b was obtained by summing up the values of s with respect to those boxes for which all the initial conditions escape and dividing the result by the number of boxes N_b for which all initial conditions escape. The boundary basin entropy was obtained in the same way, but excluding from the statistics those boxes for which either $p_1 = 0$ or $p_2 = 0$, i.e. there were considered only those boxes which have at least one boundary in their interior. The quantity S_{bb} is the summation of the entropy S for all boxes that contain at least one boundary divided by the number N_{bb} of boxes having at least one boundary.

In Fig. 10 we plot the values of the basin entropy S_b and the basin boundary entropy S_{bb} for the case of two exits, namely the wall at $x = 0$ (red points) and a small square box with center at $x = \pi/2$ and $y = 3\pi/2$ and width 0.05 (green points).

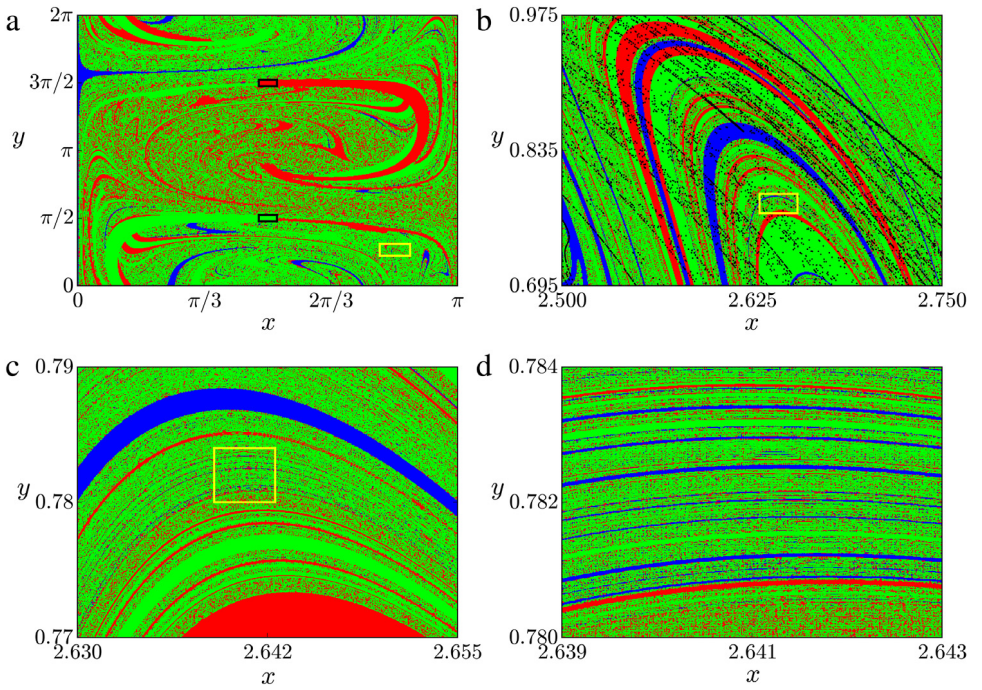

Fig. 11. Exit basins for the wall ($x = 0$, blue points) and two small boxes at $y = \pi/2$ (green points) and $y = 3\pi/2$ (red points) with both widths equal to 0.15 and for the same parameter values considered in Fig. 2(a)–(d). (b) and (d) represent successive magnification of boxes. In (b) the black line is a piece of the unstable manifold of a fixed point embedded in the chaotic region. (For interpretation of the references to color in this figure legend, the reader is referred to the web version of this article.)

The variable parameter is the amplitude of the second wave A_2, all the remaining parameters being unchanged. We also plot in Fig. 10 the fraction occupied by the red basin. The basin entropy and the basin boundary entropy follow the variation of the fraction occupied by the red basin (escape at the wall). As a general trend, the degree of complexity of the basin structure and its boundary increases with A_2, confirming that the increase of complexity of the basins is essentially due to the increase of the area of the escape basin.

6. Wada exit basin boundaries

When there are three or more exit basins, the so-called Wada property can also be observed. This is an even stronger statement of complexity than the fractality of the basin boundary for two exit basins. We begin with some mathematical definitions [34,35]: a point P is a boundary point of an exit basin $\mathcal{B}$ if every open neighborhood of P intersects the basin $\mathcal{B}$ and least another basin. The basin boundary is the set of all boundary point of that basin. The boundary point P is also a Wada point if every open neighborhood of P intersects at least three different basins. A basin boundary is said to possess the Wada property if every boundary point of $\mathcal{B}$ is a Wada point, such that the boundary of such a basin is a Wada exit basin boundary [15,24].

The presence of Wada boundaries have important physical consequences, since in this case any boundary point turns to be arbitrarily close to points of all exit basins [14]. Since an initial condition is always known up to a given uncertainty, such an uncertainty ball typically contains points belonging to all exit basins. Hence it is not possible to say with certainty to which exit basin will the trajectory asymptote to, even if we could improve the uncertainty. This would be called an extreme final-state sensitivity.

In order to look for Wada property in our system it is necessary to include a third exit, namely another square box at the same x-coordinate as the former and the same width, but its y-coordinate is displaced by π. In Fig. 11(a) we plot the basin of the first exit box (red points), the basin of the second exit box (green points) and the basin of the wall (blue points). The Wada property is can be illustrated by successive magnification of a rectangle containing pieces of the three exit basins, showing that stripes of all basins coexist in increasingly finer scales [Fig. 11(b)–(d)].

Although highly compelling, this visual evidence is not a bona fide proof that Wada property exists in this system. A necessary (but not sufficient) condition for the Wada property to exist is that the unstable manifold $W^u(P)$ of an unstable periodic orbit P belonging to this boundary must intersect every exit basin [35]. This has been shown to be true in Fig. 11(b), where we plot (in black) a segment of the unstable manifold stemming from a saddle point belonging to an exit basin boundary, which is seen to intercept points of the red, green and blue basins. Since the unstable manifold of a periodic orbit P belonging to an exit basin boundary has intersected all the exit basins the Wada property is fulfilled.

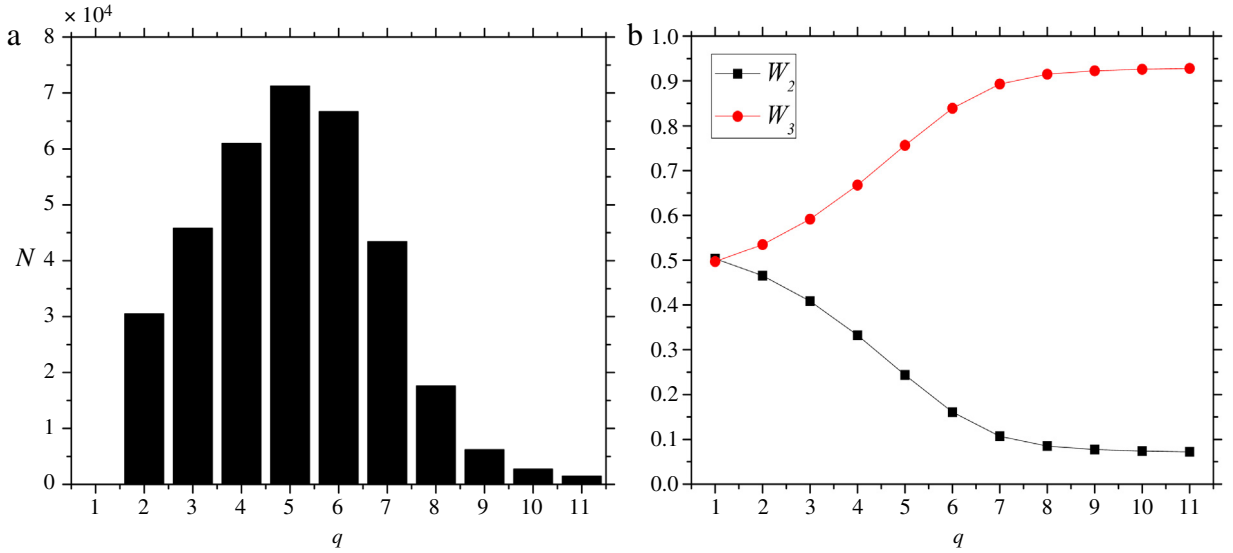

Fig. 12. (a) Number of reclassified points in each refinement step, using the grid approach for the basin structure depicted in Fig. 11. (b) Values of W_2 and W_3 as a function of the refinement step.

It has been recently proposed by Daza et al. a method for quantifying the Wada property in basin boundaries of dynamical systems (dissipative or conservative) [24]. In the following we shall indicate the basics of this grid approach as applied to escape Wada basins, further details being found in Ref. [24]. Let us consider a bounded region Ω of the phase space containing $N_A \geq 3$ disjoint escape basins S_j, where $j = 1, 2, \ldots, N_A$. There is also a two-dimensional rectangular grid G covering Ω, such that there is a set of non-overlapping grid boxes $P = \{box_1, box_2, \ldots, box_K\}$. For each point $x \in \Omega$ we assign an integer-valued "color" function C such that $C(x) = j$ if $x \in S_j$ and $C(x) = 0$ if x does not belong to any of the sets S_j, in such a way that an escape is labeled by $C(x)$.

The collection of grid boxes consisting of box_j and all the grid boxes having at least one point in common with box_j is denoted $b(box_j)$. For each box box_j we call $M(box_j)$ the number of different colors in $b(box_j)$. Provided $M(box_j) \neq 1, N_A$ we select the two closest boxes in $b(box_j)$ with different colors and draw a line segment between them, computing the color of the segment midpoint. If the computed color completes all colors inside $b(box_j)$ then $M(box_j) = N_A$ and the procedure is stopped. Otherwise we refine the procedure by choosing intermediate points until $M(box_j) = N_A$ (or the number of points exceeds a specified maximum limit).

Let G_m be the set of all the original grid boxes such that $M(box_j) = m$. If $m = 1$ then the set G_1 contains points belonging to the interior of the jth basin, because all the boxes inside the ball $b(box_j)$ have the same color. For $m = 2$ it turns out that G_2 belongs to the boundary between two basins, since there are two different colors inside the ball $b(box_j)$, and so on. We call G_n^q the set G_n at the qth procedure step. Then we compute the following parameter

$$W_m = \lim_{q\to\infty} \frac{\text{number of points of } G_m^q}{\sum_{j=2}^{N_A} \text{number of points of } G_j^q}, \tag{12}$$

where $m \in [2, N_A]$. In the limiting cases of $W_m = 0$ then the system has no grid boxes that belong to the boundary separating m escape basins, and if $W_m = 1$ then all the boxes in the boundary separate m escape basins. If $W_{N_A} = 1$ the system possesses the Wada property, since it will always be possible to find a third color between the two other two colors. The case of $0 < W_m < 1$ with $m \geq 3$ is said to be partially Wada.

In the example depicted in Fig. 11 there are three exits, hence $N_A = 3$. We divided the escape basin structure into boxes, each of them containing one point of the basin. We classify that point by analyzing the eight neighbor boxes. If all those boxes are of the same color than the central box, the latter will belong to the set G_1. If there are boxes of a same color but different from the central box, the latter will belong to G_2. If the neighbor boxes present two other colors, the central box will belong to G_3. According to (12) we compute the quantity

$$\hat{W}_2 = \frac{\text{number of points of } G_2}{\text{number of points of } G_2 + \text{number of points of } G_3} \tag{13}$$

for q procedure steps. In each refinement step we check whether or not points of G_2 may belong to G_3 by testing q initial conditions intermediate between the central box and a neighbor box of different color. If some of those q intermediate initial conditions exhibit the missing third color, the central box will be reclassified as G_3.

The number of points classified as G_3 for each refinement step q is shown as a frequency histogram in Fig. 12(a). It is apparent that after $q = 11$ refinement steps the number of reclassified points is so small that the method converges for

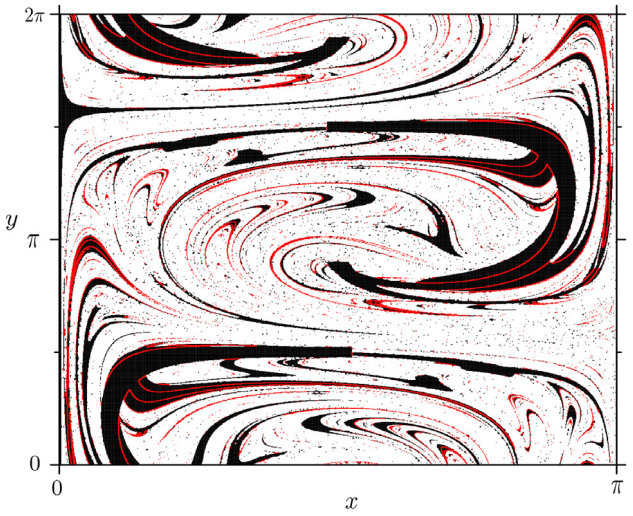

Fig. 13. Basin structure of Fig. 11, showing in black points belonging to G_1 set (internal points) and in red points of the G_2 set (boundary points), after $q = 11$ refinement steps. The points of G_3 (Wada points) are not shown for clarity. (For interpretation of the references to color in this figure legend, the reader is referred to the web version of this article.)

this value of q. This convergence can also be observed to occur both for W_2, computed from Fig. 12(b), as well for W_3, which converge to 7.2% and 92.8%, respectively. Since $0 < W_2 < 1$ the basin structure in Fig. 11 can more properly be classified as partially Wada (remember that the basin will be totally Wada if $W_2 \to 0$ if $q \to \infty$).

Fig. 13 shows in black the points classified as G_1 (internal to some basin) and in red those points that, after $q = 11$ refinement steps continue to be classified as G_2, hence belonging to basin boundaries. It is clear that some of the boundary regions really do not exhibit the Wada property, although most of the points (not shown in Fig. 13) belong to G_3, what explains why the basin structure as a whole is partially Wada.

7. Conclusions

Open non-integrable Hamiltonian systems having two or more exits allow for a detailed investigation of the complicated structure underlying the chaotic dynamics. In physical terms, it means at least two important consequences: (i) the transport in the chaotic region is far from being uniform, presenting escape channels by which particles have a faster transport rate; (ii) there is final-state sensitivity: an initial condition having a given uncertainty close enough to the basin boundaries is uncertain in the sense that we cannot be sure to what exit this initial condition will asymptote to.

Previous works in systems of interest in plasma physics have investigated this exit basins structure for the magnetic field lines in time-independent systems. In this work we have investigated the presence of exit basins with a complicated boundary structure in a time-dependent problem, which is the $\mathbf{E} \times \mathbf{B}$ drift motion of charged particles under the action of two drift waves with different amplitudes. Although our model is physically simple (the magnetic field, for example, is supposed to be uniform) we claim that the general aspects of more detailed models would be similar, in the sense that the structures we investigated are rather universal consequences of the dynamics underlying chaotic orbits in non-integrable area-preserving systems.

We observed that the exit basins closely follow the invariant manifold structure underlying the dynamics of the area-filling chaotic orbit. The exit basin boundaries are made of branches of invariant (unstable and stable) manifolds stemming from unstable periodic orbits (saddles in two dimensions) embedded in the chaotic region. For two exit basin we have shown that the boundary is indeed fractal, with a box-counting dimension close to the dimension of the phase space itself, i.e. it is almost an area-filling curve, showing the extremely involved nature of the basin structure. The box-counting dimension has been shown to increase with the amplitude of the second wave. The area occupied by the exit basins, on the other hand, has been shown to increase with the increase of the exit widths.

Moreover we applied in this paper the method of basin entropy, proposed by Daza and coworkers [13] to quantify the basin structure of any system, yielding a more direct measure to compute the loss of information on the final state of the system. In addition we found that both the basin and basin boundary entropies depend on the perturbation strength in the same way as the fraction in phase space occupied by the basin of the initial conditions leading to an escape through the tokamak wall. Since the latter generates orbits that spend a relatively large time in the chaotic region, it can be related to an enhanced radial transport of energetic particles through the tokamak wall.

In the case of three basins we also shown the Wada property to exists, thanks to the fact that the unstable manifold of an orbit belonging to the basin boundary intercepts pieces of all exit basins. We also applied a new procedure for the quantification of the basin boundary structure (grid approach) recently proposed by Daza and coworkers [24]. Our results

show that most points of the basin structure possess the Wada property, but there are phase space regions in which this property does not hold. As a consequence our basin structure is only partially Wada.

Acknowledgments

The authors would like to thank useful discussions with Dr. F. A. Marcus. This work has been supported by grants from CNPq and CAPES.

References

[1] W. Horton, Turbulent Transport in Magnetized Plasmas, World Scientific, Singapore, 2012.
[2] R. Balescu, Aspects of Anomalous Transport in Plasmas, CRC Press, 2005.
[3] W. Horton, Rev. Modern Phys. 71 (1999) 735.
[4] G. Schmidt, Physics of High-Temperature Plasmas, Academic Press, New York, 1979.
[5] W. Horton, Plasma Phys. Control. Fusion 27 (1985) 937.
[6] A.M. Batista, I.L. Caldas, S.R. Lopes, R.L. Viana, W. Horton, P.J. Morrison, Phys. Plasmas 13 (2006) 042510.
[7] S. Bleher, C. Grebogi, E. Ott, R. Brown, Phys. Rev. A 38 (1988) 930.
[8] H. Alt, H.-D. Gräf, H.L. Harney, R. Hofferbert, H. Rehfeld, A. Richter, P. Schardt, Phys. Rev. E 53 (1996) 221.
[9] J. Aguirre, M.A.F. Sanjuán, Phys. Rev. E 67 (2003) 056201.
[10] R. Barrio, F. Blesa, A. Serrano, New J. Phys. 11 (2009) 053004.
[11] J. Aguirre, R.L. Viana, M.A.F. Sanjuan, Rev. Modern Phys. 81 (2009) 333.
[12] S.W. McDonald, C. Grebogi, E. Ott, J.A. Yorke, Physica D 17 (1985) 125.
[13] A. Daza, A. Wagemakers, B. Georgeot, D. Guéry-Odelin, M.A.F. Sanjuán, Sci. Rep. 6 (2016) 3416.
[14] J. Kennedy, J.A. Yorke, Physica D 51 (1991) 213.
[15] L. Poon, J. Campos, E. Ott, C. Grebogi, Internat. J. Bifur. Chaos 6 (1996) 251.
[16] J. Aguirre, M.A.F. Sanjuán, Physica D 171 (2002) 41.
[17] Y. Zhang, H. Zhang, W. Gao, Nonlinear Dynam. 79 (2015) 2667.
[18] Y. Zhang, H. Zhang, Nonlinear Dynam. 79 (2015) 2309.
[19] J. Aguirre, J.C. Vallejo, M.A.F. Sanjuán, Phys. Rev. E 64 (2001) 066208.
[20] F. Blesa, J. Seoane, R. Barrio, M.A.F. Sanjuán, Internat. J. Bifur. Chaos 22 (2012) 1230010.
[21] Z. Toroczkai, G. Károlyi, A. Péntek, T. Tél, C. Grebogi, J.A. Yorke, Physica A 239 (1997) 235.
[22] A. Péntek, Z. Toroczkai, T. Tél, C. Grebogi, J.A. Yorke, Phys. Rev. E 51 (1995) 4076.
[23] U. Feudel, A. Witt, Y.-C. Lai, C. Grebogi, Phys. Rev. E 58 (1998) 3060.
[24] A. Daza, A. Wagemakers, M.A.F. Sanjuán, J.A. Yorke, Sci. Rep. 5 (2015) 16579.
[25] E.C. da Silva, I.L. Caldas, R.L. Viana, M.A.F. Sanjuán, Phys. Plasmas 9 (2002) 4917.
[26] T.E. Evans, R.K.W. Roeder, J.A. Carter, B.I. Rapoport, Contrib. Plasma Phys. 44 (2004) 235.
[27] J.S.E. Portela, I.L. Caldas, R.L. Viana, M.A.F. Sanjuán, Internat. J. Bifur. Chaos 17 (2007) 4067.
[28] R.L. Viana, E.C. da Silva, T. Kroetz, I.L. Caldas, M. Roberto, M.A. Sanjuán, Phil. Trans. R. Soc. A 369 (2011) 371.
[29] R.S. Oyarzabal, J.D. Szezech Jr., A.M. Batista, S.L.T. de Souza, I.L. Caldas, R.L. Viana, M.A.F. Sanjuán, Phys. Lett. A 380 (2016) 1621.
[30] T. Kroetz, F.A. Marcus, M. Roberto, I.L. Caldas, R.L. Viana, E.C. da Silva, Comput. Phys. Comm. 180 (2009) 642.
[31] A.F. Marcus, T. Kroetz, M. Roberto, I.L. Caldas, E.C. da Silva, R.L. Viana, Z.O. Guimarães-Filho, Nucl. Fusion 48 (2008) 024018.
[32] Z.O. Guimaraes-Filho, I.L. Caldas, R.L. Viana, M.V.A.P. Heller, I.C. Nascimento, Yu.T. Kuznetsov, R. Bengtson, Phys. Plasmas 15 (2008) 062501.
[33] C. Grebogi, S.W. McDonald, E. Ott, J.A. Yorke, Phys. Lett. A 99 (1983) 415.
[34] H.E. Nusse, J.A. Yorke, Science 271 (1996) 1376.
[35] H.E. Nusse, J.A. Yorke, Physica D 90 (1996) 242.